MABS
2025, VOL. 17, NO. 1, 2599580
https://doi.org/10.1080/19420862.2025.2599580

Taylor & Francis
Taylor & Francis Group

REPORT

OPEN ACCESS Check for updates

Functional NK engagers from OmniClic, a common light-chain platform producing fully human-sequence antibodies in a chicken host species

Baisen Zeng[a], Ingrid Mechin[a*], David Mowrey[a*], Gerry S Rivera[a*], Hunter G Nyvall[b,c], Sushant Suresh[b], John E Burke[b,c,d], William Harriman[a], Bob Chen[a], and Yasmina Abdiche[a]

[a]OmniAb, Inc ., Emeryville, CA, USA; [b]Department of Biochemistry and Microbiology, University of Victoria, Victoria, BC, Canada; [c]Department of Biochemistry and Molecular Biology, The University of British Columbia, Vancouver, BC, Canada; [d]University of Victoria Genome BC Proteomics Centre, Victoria, BC, Canada

ABSTRACT

Next-generation antibodies include a growing number of bispecific and multispecific antibodies that are commonly used to redirect the immune system to fight cancer. Herein, we assessed the depth and breadth of epitope coverage as a proxy for functional diversity in human immune repertoires produced by two complementary *in vivo* platforms utilizing a common light chain, in a chicken (OmniClic™) or rat (OmniFlic®) host species. We adopted NKp46 as a model to target antigen due to its use in emerging natural killer (NK) immune engagers that are being explored clinically as potentially safer alternatives to traditional CD3-based T cell engagers. To probe the epitope diversity of our antibody repertoires, we performed a detailed high throughput epitope binning study using surface plasmon resonance and corroborated our binning assignments with epitope mapping data deduced from hydrogen deuterium exchange mass spectrometry. Our results revealed broad epitope coverage and nuanced diversity both within and across repertoires, with few epitopes shared, suggesting that the complementary use of OmniClic™ and OmniFlic® produces more comprehensive coverage than either alone. Furthermore, our epitope binning assignments aligned with our complementarity-determining region-based sequence lineage assignments, enabling a direct comparison of sequence diversity across Clic and Flic repertoires despite their use of different scaffolds, a single functionally rearranged V(D)J scaffold versus multiple combinatorially assembled V(D)J scaffolds, respectively. The rich epitope diversity of both OmniClic™ and OmniFlic® yielded multiple candidates for functional NK activators, as determined in an antibody-dependent cellular cytotoxicity assay, demonstrating their value as building blocks in constructing optimized immune engagers.

ARTICLE HISTORY
Received 21 October 2025
Revised 28 November 2025
Accepted 1 December 2025

KEYWORDS
ADCC; antibody; epitope binning; HDX-MS; machine learning; NGS; NKp46; SPR

Introduction

Therapeutic antibodies have revolutionized medical treatment options for patients, especially those suffering from cancer and autoimmune disorders[1–3]. Compared with other drug modalities, antibodies offer advantages of exquisite specificity, high affinity, and long serum half-life, minimizing the dose and frequency of dosing needed to produce a safe and efficacious response in patients[4]. Antibodies can be used in various ways to bring therapeutic benefit to patients, and this is reflected in the myriad of molecular formats in approved and clinical-stage drugs, as driven by the intended biological mechanism of action[5].

The molecular and functional diversity of antibodies is further expanded by the increasing number of bispecifics that have been approved in recent years[6–8] fueled by a robust clinical pipeline with emerging multi-specifics[9–12]. A major mechanism of action for approved bispecifics is immune cell engagement, a type of immunotherapy where the antibody helps the body to fight cancer[13,14]. In this type of bispecific antibody, one specificity recruits an immune cell, typically a T cell via the CD3 receptor on its surface, and the other redirects it to a tumor cell, via tumor-associated receptors such as EpCAM, CD19, CD20, BCMA, GPRC5D, or DLL3, thereby mobilizing immune cells directly to the tumor site where they activate immune cell-mediated anti-tumor immune responses, while sparing healthy cells.

CONTACT Yasmina Abdiche yabdiche@omniab.com OmniAb, Inc., 5980 Horton Street, Suite 600, Emeryville, CA 94608, USA
*These authors contributed equally.
Supplemental data for this article can be accessed online at https://doi.org/10.1080/19420862.2025.2599580.

© 2025 The Author(s). Published with license by Taylor & Francis Group, LLC.
This is an Open Access article distributed under the terms of the Creative Commons Attribution-NonCommercial License (http://creativecommons.org/licenses/by-nc/4.0/), which permits unrestricted non-commercial use, distribution, and reproduction in any medium, provided the original work is properly cited. The terms on which this article has been published allow the posting of the Accepted Manuscript in a repository by the author(s) or with their consent.

Most approved anti-CD3 bispecifics are used to treat blood cancers such as lymphoma, myeloma, and leukemia, with limited success achieved in treating solid tumors[15–17]. As a drug class, use of CD3-directed bispecifics is often hampered by significant dose-limiting toxicities, especially cytokine release syndrome[18]. The design of CD3 engagers continues to evolve to overcome these challenges by optimizing the antibody's binding affinity, valency, epitope specificity including logic gating and targeting specific T cell subsets, conditional activation, and molecular geometry, among other considerations[19]. As an alternative to T cell engagers, next-generation clinical-stage immune engagers are also exploring the use of other types of immune cells such as natural killer (NK) cells[20] that can be targeted via activating receptors such as CD16a and NKp46[21,22].

Since 'one size does not fit all' when optimizing the molecular format of a bispecific and multi-specific antibodies[10], technologies that facilitate the combination of disparate variable antibody domains as building blocks for custom molecular constructs are appealing. Within the engineering toolbox used to assemble biotherapeutics are common light chain (cmLC) antibodies[23], an elegant approach that eliminates the light-chain mispairing problem of traditional IgG-like bispecifics and facilitates their manufacture[24] without compromising target-binding affinity[25]. The blockbuster drug emicizumab (Hemlibra®), which represents the first cmLC bispecific antibody to be approved by the Food and Drug Administration (in 2017), has transformed the treatment options for the clinical management of hemophilia A[26]. Several cmLC antibodies are in clinical development[27,28]. An under-appreciated but substantial practical convenience of cmLC antibodies is in the screening stages of a de novo discovery campaign because they obviate the need to preserve native heavy and light-chain pairing, and thereby reduce selections to just the native heavy chain variable domain, which has been optimized to pair with a germline cmLC.

We set out to explore the binding kinetics, affinity, epitope diversity, developability, and biological functional activity of antibodies from the immunization of OmniClic™ (abbreviated as 'Clic') animals, a cmLC platform producing fully human-sequence immune repertoires in a chicken host, which is a divergent, single-scaffold gene-converting species[29]. We benchmarked our results against immunization of OmniFlic® (abbreviated as 'Flic') animals, a cmLC platform that produces fully human-sequence immune repertoires in a rat host species and is an established industry standard used in clinical-stage CD3-bispecifics : etentamig (CD3 X BCMA)[30] and surovatamig (CD3 X CD19)[31]. As a model target, we chose NKp46, an activating receptor on NK cells that has gained popularity in clinical-stage multi-specific immune engagers[21,32]. We posit that NKp46 antibodies from our immune repertoires showing functional activation could be reformatted as bispecific or multispecifics to provide versatile options for constructing next-generation immune engagers.

Results

OmniClic and OmniFlic repertoires produce comparably diverse kinetics and affinities

NKp46-specific antibodies generated from protein immunizations of Clic and Flic animals were isolated in a single B cell workflow using the xPloration® instrument, a microcapillary-based array screening system[33], and tested for their target-binding kinetics and affinities by surface plasmon resonance (SPR). Initial phenotypic selections yielded a similar number of unique-sequence clones from each repertoire (44 Flic and 45 Clic) with diverse-binding kinetics and affinities spanning a similar range, with K_D values from 0.5 nM to 200 nM, with many showing K_D values comparable to the benchmarks, which were single-digit nM (Figure 1a,b, and S1 Fig).

Variational autoencoder-based hit expansion retrieved higher affinities than those from phenotypic selections

To retrieve even higher affinity clones than those from our phenotypic selections, we performed a data-driven antibody hit expansion of Clic repertoires using a variational autoencoder (VAE) trained on next-generation sequencing (NGS) data from the same immunized antibody repertoires. Artificial intelligence (AI)-expanded hits were, on average, 10-fold higher affinity than those from our original phenotypic selections. This improvement can be seen in the iso-affinity plot and K_D scatter plot shown in Figures 1a,

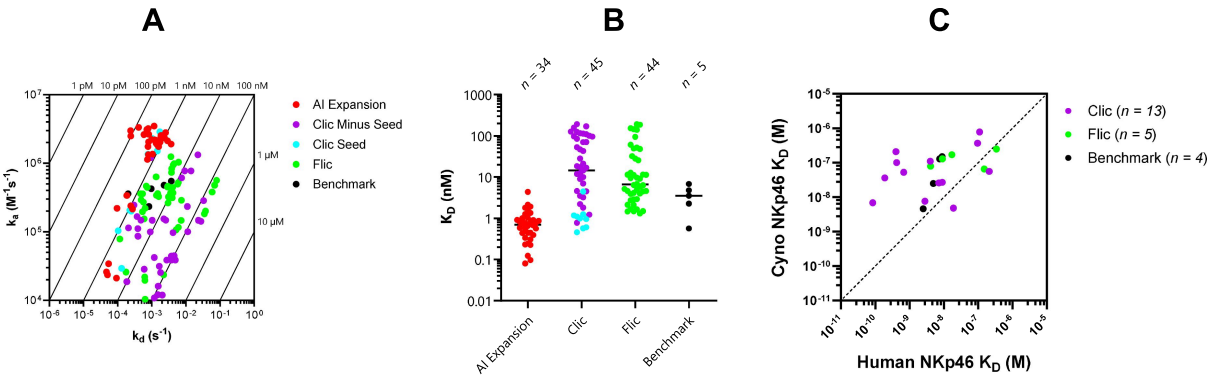


Figure 1. Binding kinetics and affinities for human NKp46. (A) Isoaffinity plot and (B) Scatter plot for human NKp46 affinity determinations of Clic (AI-expanded hits; original with or without 'seeds,' which are clones selected for AI hit-expansion based on their high-affinities), Flic, and benchmarks (see S1 table). (C) Scatter plot of binding affinities for human NKp46 compared with cyno NKp46 for a subset of clones (see S2 table). In panel C, Clic clones from original, seed, and AI-hit expansion are treated as one 'repertoire.' Data in panels A and B were determined using in-house-produced NKp46, whereas data in panel C was determined using commercially sourced (Acro) proteins.

b, respectively, where AI-expanded hits (in red) 'burst' from the 'seeds' (in cyan) giving slower dissociation rate constants, resulting in lower K_D values. Additionally, we selected a subset of clones for binding affinity to cynomolgus (cyno) NKp46 (sharing 86% identity with human NKp46) and found many cyno cross-reactive clones within both Clic and Flic repertoires. We also found examples of human-specific NKp46 clones that did not cross with cyno NKp46 (see S2 Table).

Clic and Flic repertoires show broad and complementary epitope coverage

We performed a detailed and statistically powered high-throughput (HT) epitope binning study on a merged panel of clones from Clic and Flic repertoires to assess the breadth and depth of their epitope coverage. We incorporated a small panel of literature clones (Innate-1, 2, 3, 4, and 9)[32] as benchmarks to determine whether our antibodies could overlap known epitopes and expand coverage beyond them. Of these five benchmarks, two (Innate-1 and Innate-4) served as structural benchmarks (PDB:6IAP). Innate-1, 2, 3, and 4 reportedly target distinct, non-overlapping epitopes, which we empirically confirmed (S2 Fig). Innate-2 and Innate-9 reportedly overlap with one another. We also included three previously described single domain heavy chain-only antibodies (OmnidAb® clones, herein called 'dAbs') as tool compounds defining the Innate-3 epitope[34].

Figure 2 shows network plots from an epitope binning analysis of 119 total clones comprising 70 Clic (including expanded hits), 41 Flic, five benchmarks, and three dAbs. In a network plot, each node is a unique antibody and each chord connecting two nodes suggests a blocking relationship between the two antibodies. It is assumed that all antibodies have been tested against one another in a combinatorial pairwise manner such that the absence of a connecting chord between two nodes indicates the lack of a blocking relationship, which is detected in our so-called "classical sandwich" epitope binning assay format, as the formation of a ternary or "sandwich" complex, due to the binding of a solution antibody (as analyte) to NKp46 that is first tethered by an immobilized antibody (as ligand) on our SPR chip surface. Based on the observed (or in some cases, inferred) blocking relationships (see Methods), antibodies are clustered into epitope groups. To determine an appropriate clustering level, we first assigned clones to five groups or 'super-communities' and named them (1 through 5) based on their blocking relationships with the benchmarks (Innate-1, 2, 3, 4 and none); these were then split into more granular groupings to give a total of 14 'communities,' as shown by the network plot in Figure 2a that is colored by community.

Table 1 lists the 14 assigned epitope communities and how they were populated by Clic, Flic, and the benchmarks. The four benchmarks (Innate-**1**, Innate-**2**, Innate-**3**, and Innate-**4**) were thus assigned to four discrete communities (Com-**1**, Com-**2**a, Com-**3**, and Com-**4**a) with Innate-2 and Innate-9 sharing the same community. Despite their non-overlapping epitopes, Innate-1 and Innate-4 epitopes were strongly

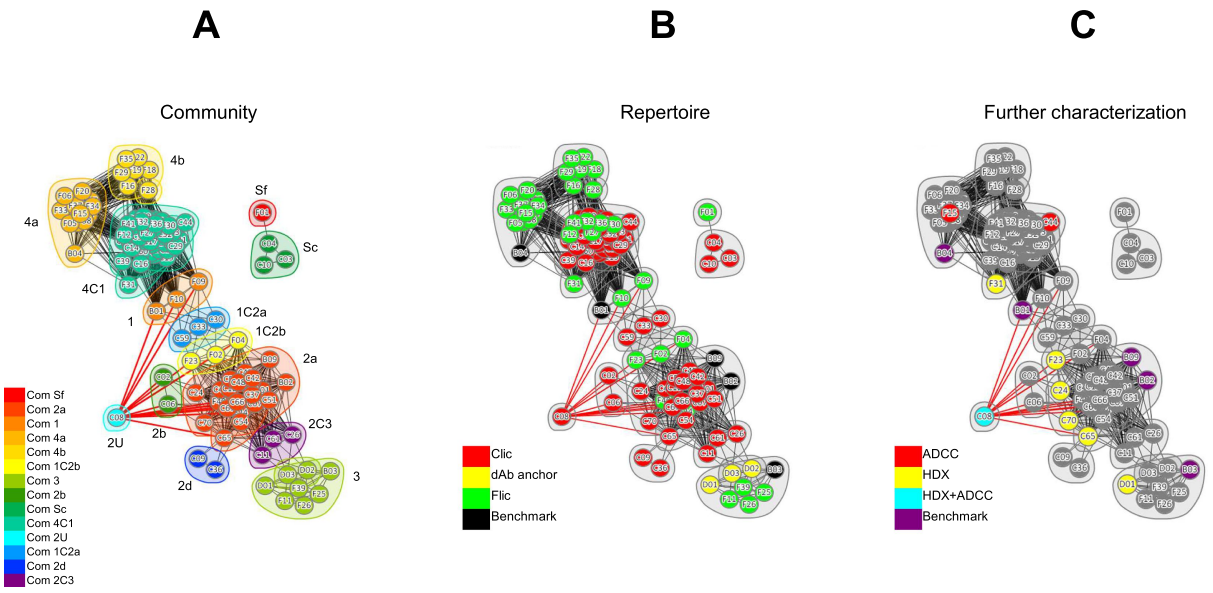


Figure 2. Epitope binning network plots. Plots are colored by (A) Community, (B) Repertoire, or (C) Clones selected for further characterization. See S3 fig for binning heat maps and dendrograms.

Table 1. Epitope communities and their distribution within and across repertoires.

Community	Repertoire
Com 1	Flic + Innate-1
Com 1C2a	Clic
Com 1C2b	Flic
Com 2a	Clic + Flic + Innate2 + Innate-9
Com 2b	Clic
Com 2C3	Clic
Com 2d	Clic
Com 2U	Clic
Com 3	Flic + Innate-3
Com 4a	Flic + Innate-4
Com 4b	Flic
Com 4C1	Clic + Flic
Com Sc	Clic
Com Sf	Flic

Community names are based on their blockade of benchmarks: Com 1, 1C2a, and 1C2b are related to Innate-1; Com 2a, 2b, 2c3, 2d, and 2U are related to Innate-2; Com 3 blocks Innate-3; and Com 4a, 4b, and 4C1 is related to Innate-4. Com Sc (Clic-only) and Sf (Flic-only) are special communities that do not block any benchmark. Capital letter 'C' in the community's name indicates a community that 'connects' two otherwise non-overlapping communities. See S1 Table for community assignments for all clones tested.

overlapped by a large group of clones, likely due to immunogenicity of those epitopes and our Clic AI hit-expansion that focused on four communities (1, 4a, 4b, and 4C1). Three Flic clones fall into the Innate-3 community (Com-3), anchored by our Innate-3-like dAb clones. We identified a Special epitope cluster distinct from and non-overlapping with the benchmark comprising Flic (Com-Sf) and Clic (Com-Sc) clones. Another novel epitope cluster connecting Innate-1 and Innate-2 is composed Com-1C2a and Com-1C2b. Of the 14 defined communities, six were Clic-only and six were Flic-only with two shared across Clic and Flic (Table 1). As observed in Figure 2b, where the nodes are colored by repertoire, Flic recapitulated the epitopes of all benchmarks tested, while Clic only recapitulated that of Innate-2 (which fell into the same community as Innate-9). Taken together, Clic and Flic produced clones that blocked the benchmarks in many ways as seen by the complex network of chords emanating from the benchmarks connecting Clic and Flic clones that cross-talked across communities. Additionally, Clic and Flic accessed

epitopes not represented by the benchmarks, as shown by nodes that have no chords (no blocking relationships) connecting them to any benchmarks.

Detailed epitope binning studies reveal nuanced epitope diversity that is corroborated by epitope mapping

To justify the community-level grouping of our SPR-based high throughput binning approach, hydrogen deuterium eXchange mass spectrometry (HDX-MS) was used to epitope-map a subset of clones. HDX-MS measures the exchange rate of amide hydrogens, with this rate primarily dependent on secondary structure stability, making it well suited to capturing changes conformational dynamics induced by antibody–antigen interactions[35,36]. Differences in deuterium exchange were deemed significant if they fulfill all the following criteria: percent difference greater than 5%, difference in number of deuterons incorporated greater than 0.4 and p-value less than 0.01 after applying a two-tailed T-Test (n = 3). The peptide coverage of NKp46 was ~40%, with any epitopes present in these regions being unmappable. This is not uncommon in heavily disulfide-linked proteins[37]. Despite these challenges, we were able to define conformational differences in NKp46 upon binding to distinct classes of antibodies. When interpreting HDX-MS results, understanding that differences can be caused by direct-binding interactions (epitopes), but also by allosteric conformational changes, is critical. To explore epitope breadth, we chose clones from distinct epitope communities (1C2b, 2a, 2 U, 3, and 4C1) and, to explore epitope depth, we chose clones from the same community (2a) showing highly similar blocking profiles. The alignment across our binning and HDX-MS mapping studies reinforced the reliability of our binning experiments (Table 2).

Figure 3 shows examples of three clones mapped via HDX-MS superposed with deduced epitopes from structural benchmarks Innate-1 and Innate-4 (PDB:6IAP): F31 (Com 4C1), C24 (Com 2a), and D01 (Com 3). The blocking relationships from SPR binning experiments via pairwise combinatorial antibody competition are shown as chords in the community network plots and can be used to explain the HDX-MS mapping data. Visual navigation of the community network plot is facilitated by comparing Figure 2a (colored by community) with Figure 2c (colored by the clones selected for further characterization). See S4 Fig for the mapped epitopes deduced for each antibody tested.

The binning data suggests that clone F31, a member of Com-4C1, competes with Innate-4 (B04) but not with Innate-1 (B01). HDX-MS data identifies residues *L39-F62* as protected upon engagement of antibody F31 with NKp46 (Figure 3a). This protection profile aligns with the B04 epitope (identified by PDB:6IAP) while having no overlap with the B01 epitope. This agreement between the binning and mapping data rationalizes the community assignment for antibody F31, one of the Com-4C1 clones that recognizes a large antigen surface area connecting B04 and B01 epitopes.

Table 2. Epitope mapping deduced by HDX-MS.

Clone ID	Hu K_D (nM)	Cy K_D (nM)	Com	Difference >10% (5–10%)[b]
F23	6	N/B	1C2b	*L135-Y147, S172-F180, (G148-C169)*
C65	19	4.8	2a	*S130-F132, L135-F154, S172-Y173, (P155-G171, P181-L187)*
C24	0.19	N/B	2a	*L135-Y147 (H108-F121, G148-A177)*
C70	2	N/B	2a	*L135-Y147, (G148-C169)*
C08[a]	9	27	2U	*S130-F132, G148-Y173*
D01	61	N/B	3	*H108-F121*
F15[a]	4.1	79	4a	N/T
F31	17	170	4C1	*L39-F62*
C44[a]	0.085	6.9	4C1	N/T
				Epitope Deduced from PDB:6IAP[c]
B01	2.5	4.6	1	20–21,67–70,96,98–102,104,125–127,173,180,183
B04	4.9	25	4a	35–36,38,40,43,45,48,54,76,78,80–88

Summary of clones selected for further characterization by HDX-MS and/or ADCC. See S3 Table for statistical analysis; S4 Table for NKp46 alignment showing deduced epitopes; and S1 File for source data. N/B = non-binder to cyno NKp46. N/T = not tested.

[a]Clones selected for ADCC analysis: C08 (Com 2U), F15 (Com 4a), and C44 (Com 4C1).

[b]Residues showing %D difference >10% (regions with %D difference between 5–10% shown in brackets) all listed residues also met criteria of #D difference >0.4 Da and $p<0.01$ ($n=3$). Underlined residues indicate peptide *L135-Y147* anchoring Com 2a, also present in Clone F23's epitope (Com 1C2b) 'connecting' Com 1 and Com 2.

[c]Epitopes for the structural benchmarks were deduced from PDB:6IAP within 4.5 Angstrom.

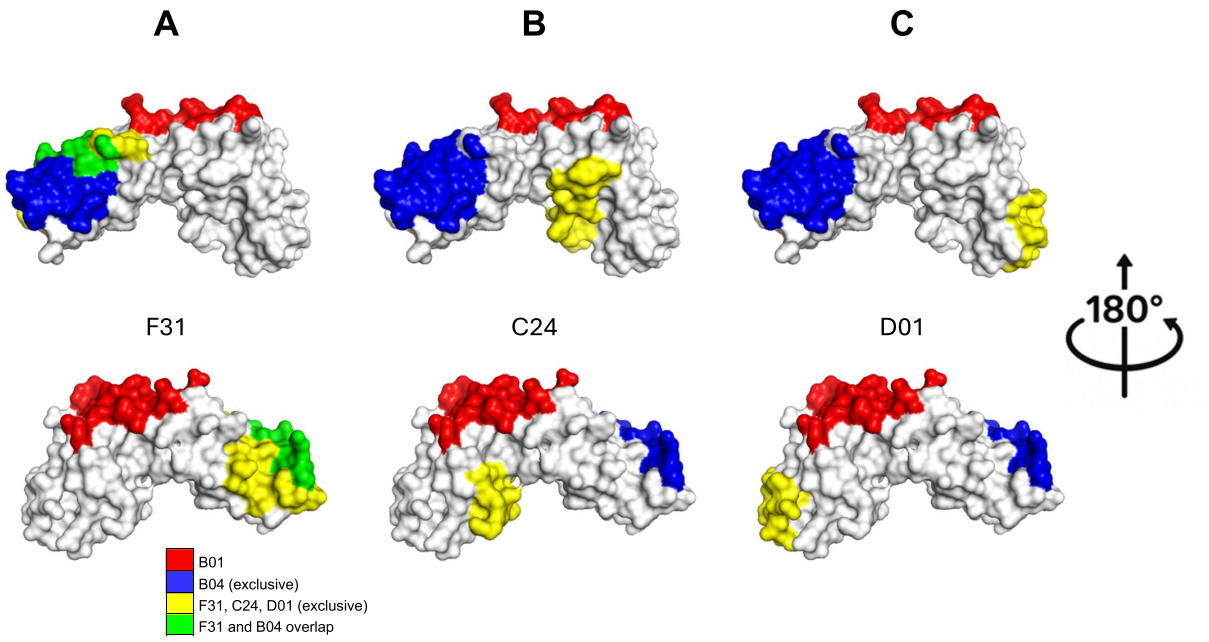


Figure 3. Epitope mapping by HDX-MS. Images of (A) F31 (Com 4C1), (B) C24 (Com 2a), and (C) D01 (Com 3) showing HDX-MS results compared with epitopes of the structural benchmarks, B01 and B04 (PDB:6IAP): red = B01, blue = B04 (exclusive), yellow = HDX-MS results of F31, C24, D01 (exclusive), mapped regions showed a decrease in exchange with %D difference >10% (also met criteria of #D difference >0.4 Da and $p<0.01$ [$n=3$]), green = NKp46 regions with HDX protection in presence of F31 which overlap with the B04 epitope.

Clic produced a unique clone, C08, that is assigned to its own community (Com-2**U**). Binning data suggests that C08 is the only clone that not only blocks select Com-2a members but also directly blocks B01, contrary to being indirectly related to B01, through Com-1C2. On the nodal plot, chords connecting C08 to its competitors are highlighted in red for ease of visualization (Figure 2c). Mapping data identifies NKp46 residues *S130-F132* and *G148-Y173* were protected upon binding to antibody C08. While no residue is shared between C08 and B04 epitopes, one residue, *Y173*, is shared between C08 and B01, which could justify the competition between C08 and B01 observed in the binning data.

In the absence of HDX-MS data for a Com-1C2a clone, we can only postulate that Com-1C2a epitope likely wedges between that of Innate-1 and Innate-2. Based on binning data, F23 belongs to Com-1C2b, which is the other community that connects Com-1 to Com-2a. Mapping data identifies residues *L135-Y147* and *S172-F180* as the regions with the most significant protection. Peptide *S172-F180* overlaps with C08 epitope at the dipeptide *S172Y173*, in line with the observation that F23 is in direct competition with C08.

C24 does not compete with B04, B01, or C08. Mapping data identifies *L135-Y147* as the regions undergoing the largest protection (Figure 3b), which does not overlap at any residue with the known epitopes of structural benchmarks or the mapped epitope of C08. At the community granularity level, both C24 and C65 are assigned to Com-2a, but they are sufficiently distinct from each other in that only C65 directly competes with C08 in binning. Mapping data identifies *S130-F132*, *L135-F154*, and *S172-Y173* as protected when NKp46 is bound by C65. This overlaps with the protection profile of C08, which showed differences at regions *S130-F132*, *G148-F154*, and *S172-Y173*.

Clone C70 competes with C61, a Com-2C3 clone that connects Com-2a and Com-3. Mapping data identifies *L135-Y147* as regions with the strongest protection (greater than 10% difference), *G148-C169* had a difference in exchange between 5% and 10%. On the PDB:6IAP structure, the *G148-C169* patch extends C70 epitope beyond *L135-Y147* and reaches toward the distal end of NKp46 C-terminal domain, which aligns with Com-3 (D01) HDX changes. C70 is the Com-2a member with a blocking profile extending closest to Com-3 yet does not directly block Com-3 clones.

Finally, we mapped a dAb clone, D01, which showed protection in residues *H108-F121*, suggesting the Com-3 epitope (co-populated by Innate-3) is localized to the distal end of the C-terminal domain of NKp46 (Figure 3c). Peptide *H108-F121* also covers a surface that immediately neighbors *G148-C169*, this region

showed a stabilization (decreased HDX) when NKp46 bound the C70 antibody. This could provide an explanation as to why C70 competes with C61, a Com-2C3 clone, in binning.

Epitope communities aligned with sequence lineage assignments

We observed agreement between antibody sequence lineage assignments and epitope binning communities in both Clic and Flic repertoires. Figure 4a shows that 70 Clic clones (including expanded hits) were assigned to 19 sequence lineages or 'clusters' and 8 epitope communities. Seed clones for our hit expansion were chosen from Com 2a and Com 4C1 and these epitope communities were preserved in expanded hits. The use of multiple birds further increased opportunities for sequence diversity, as shown by C69, C23, and C05, each from different birds converging on Com-4C1, while C36 and C09, also from different birds, both hit a rare epitope (Com-2d).

Figure 4b shows that 40 Flic clones were assigned to 16 sequence lineages covering 8 epitope communities, using multiple germlines (Figure 4c). Like Clic, the use of multiple animals contributed to the overall diversity, with some epitope communities uniquely produced by some animals, while other communities were shared across animals by convergence of disparate sequences. In this cohort, we noticed a rare case of clones assigned to the same lineage showing an epitope shift. This was seen by F28, a lineage 2 clone (red innermost color wheel in Figure 4b), whose epitope shifted to Com-4b, deviating from its lineage siblings that belong to Com-4C1 (see S3d Fig showing sensorgrams supporting this observation).

The Venn diagram (Figure 4d) and Table 1 show how the 14 epitope communities are distributed within and across Clic and Flic repertoires. Clic (70 clones, including expanded hits) uniquely populated six communities (1C2a, 2b, 2C3, 2d, 2 U, and Sc) while Flic (40 clones) also uniquely populated six communities (1, 1C2b, 3, 4a, 4b, and Sf), with only two communities shared (2a and 4C1), providing repertoire-distinct opportunities, within the sample size tested. Flic (rat host species) thus recapitulated the epitope communities of all four benchmarks (Innate-1, 2, 3, and 4: Com-1, Com-2a, Com-3, and Com-4a, respectively) likely because those were also produced by immunization of a rodent (mouse), while Clic only recapitulated one of them (Innate-2: Com-2a), but provided multiple options for other, Clic-only epitope communities, likely due to differential target recognition possible in a divergent host species. While Flic showed large sequence diversity as defined by its germline usage, Clic showed large sequence diversity in the HCDRs. As such, Clic and Flic show comparable diversity when considering epitope diversity, with complementary opportunities for epitope coverage.

Both Clic and Flic repertoires yielded functional NK engagers across various epitope communities

We next investigated whether our NKp46 antibodies could induce NK cell-mediated killing of tumor cells in an antibody-dependent cellular cytotoxicity (ADCC) assay. To enable the use of a well-established EGFR-expressing cancer cell line (A549) we formatted our NKp46 antibodies as EGFR bispecifics using a symmetrical tetravalent 2 + 2 scFv-IgG Morrison format[38], a commonly used format for producing multispecifics and among the many used in clinical-stage NK engagers[12,39] and in preclinical studies[40]. We tethered cetuximab scFv from an anti-NKp46 IgG backbone, explored two different tethering locations (at C-terminal of the heavy chain or light chain) and tested both STR-silenced (mAbsolve, see Methods for details) and active IgG1-Fc backbones to determine whether NKp46-engagement alone was sufficient to produce ADCC (on a silent Fc backbone), and whether NKp46 engagement could augment ADCC on an active Fc backbone (via the 'normal' CD16a/IgG1-Fc-mediated activation). Three clones from disparate epitope communities with similar or higher affinities than the benchmarks were selected for reformatting into EGFR bispecifics. From Clic, we chose C08 because of its unique epitope (Com 2 U) and C44 (Com 4C1) because of its high affinity and tested each of them in a different Morrison format. From Flic, we chose F15 (Com 4a) and tested it in both Morrison formats.

We first confirmed that the bispecific compounds had negligible effect on the growth of tumor target cells alone in the absence of NK cells along with appropriate controls (S5 Fig). We then tested the bispecific compounds (and vehicle, representing phosphate-buffered saline (PBS) alone) for their effect on the growth of tumor target cells co-cultured with NK cells compared with untreated co-cultures: Table 3 summarizes these results. Eight bispecific compounds were tested (Figure 5a) and split by Morrison format (HC-

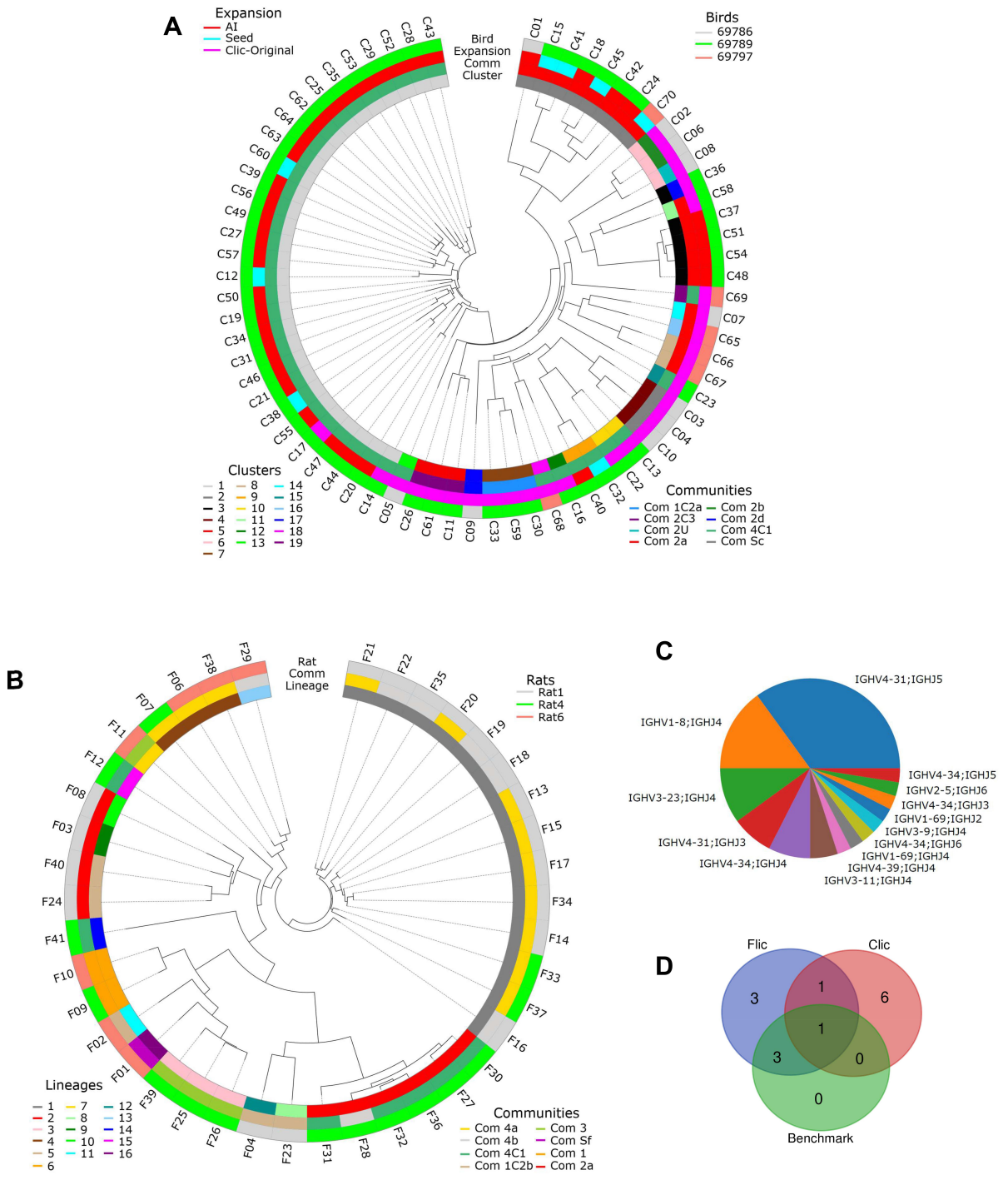


Figure 4. Sequence analysis. Circular sequence dendrograms for (A) Clic (n = 70) and (B) Flic (n = 40) repertoires merged with epitope binning data. Color wheels (inner to outer) indicate sequence lineage (or 'cluster' for Clic), epitope community, expansion (Clic only), and animal (bird or rat). (C) Pie chart showing Flic V+J germline usage. (D) Venn diagram showing how the 14 epitope communities are distributed across Clic and Flic repertoires.

tethered or LC-tethered scFv-IgG) across six total donors, using three donors per Morrison format. There was significant donor-to-donor variability. Within the first set of donors (donors 1, 2, and 3) used to test HC-tethered scFv-IgG, donor 2 appeared mostly resistant/non-responsive. Donors 4, 5, and 6 (used to test LC-tethered scFv-IgG) were generally poorer responders than donors 1, 2, 3 (S6 Fig and S7 Fig). All bispecific compounds on an active Fc backbone produced a moderate reduction in tumor cell growth, comparable to or slightly worse than cetuximab IgG control (Figure 5b). None of the active Fc bispecifics

Table 3. ADCC results.

Sample[a]	Epitope Com	Donors	ADCC Potency[b]
C08-HC-Active	Com 2U	1, 2, 3	(++)
C08-HC-Silent			(++) in 2 of 3 donors
F15-HC-Active	Com 4a		(++)
F15-HC-Silent			(+) in 2 of 3 donors
C44-LC-Active	Com 4C1	4, 5, 6	(++/+++)
C44-LC-Silent			(++)
F15-LC-Active	Com 4a		(++)
F15-LC-Silent			(+++)

[a]Sample name indicates Clone ID (C08, F15, or C44), Morrison format (Heavy Chain or Light Chain tethered scFv-IgG) and Active or Silenced Fc backbone.
[b]ADCC potency is scored as slight (+), moderate (++) or substantial (+++) reduction in tumor cell growth. Cetuximab control is (++). See S2 File for statistical analysis supporting this simple categorization.

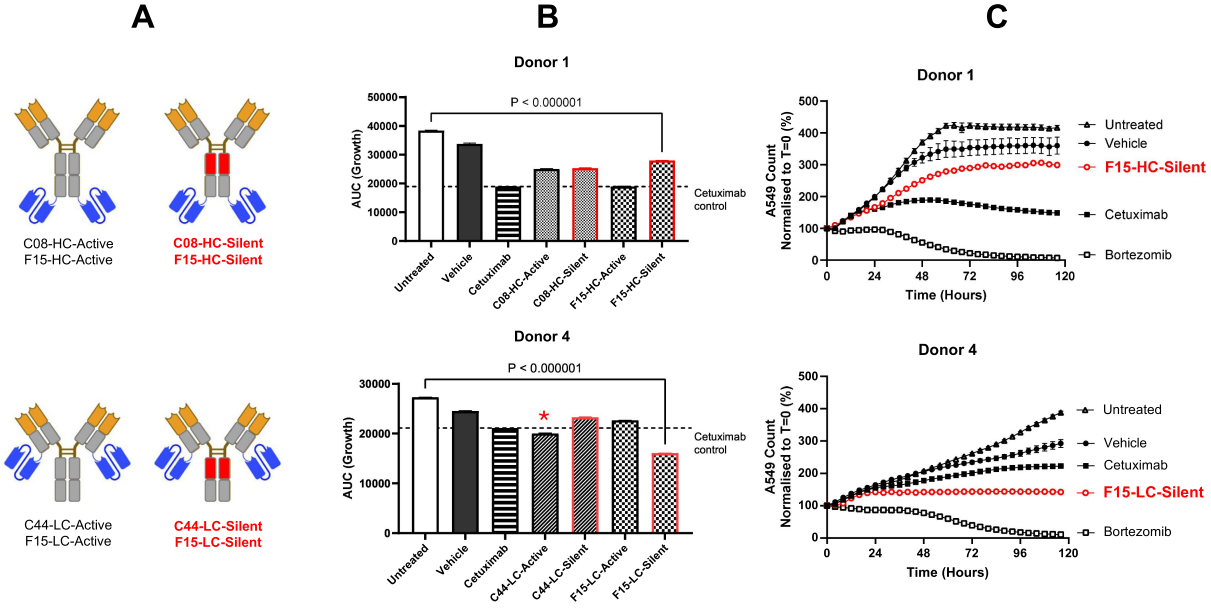


Figure 5. ADCC results. (A) Morrison formats of bispecific compounds tested. (B) IncuCyte AUC data showing tumor growth reduction for A549 cells co-cultured with NK cells upon treatment with or without vehicle (PBS), cetuximab control or bispecific compounds. Student T-test shows statistical significance of the F15-LC-Silent bispecific compound. See S2 File for statistical analysis of all samples tested. (*) C44-LC-Active showed slightly more reduction in tumor cell growth than the cetuximab control. (C) IncuCyte time-course data showing format-dependent tumor cell killing by F15 on a silent backbone, compared with controls. Panels B and C show data for one out of the three tested donors: donor 1 is representative of donors 1,2, 3 and donor 4 is representative of donors 4, 5, 6. See S5-S7 figs.

augmented tumor cell killing beyond that for the cetuximab IgG control, except LC-tethered scFv-IgG C44, which consistently appeared slightly better than the cetuximab control in all three donors tested. Since vehicle (PBS alone) showed a mild inhibitory effect, we provided two sets of statistical T-tests for each bispecific sample and cetuximab-IgG control, one comparing untreated and another comparing vehicle: see S2 File.

Comparing the tumor cell killing of silent Fc constructs to one another, all showed some reduction of tumor cell growth, with LC-tethered scFv-IgGs appearing more potent than HC-tethered scFv-IgGs (Figure 5b). This was clearly demonstrated by clone F15, which was tested in both Morrison formats. Furthermore, of all eight bispecific compounds tested, including active and silent Fc backbones, the most potent one was on a silent Fc backbone (LC-tethered scFv-IgG F15-silent), significantly outperforming its active Fc counterpart in the same format, suggesting that NKp46-engagement was sufficient to produce a greater tumor cell killing than cetuximab IgG Control, but that the geometry of the molecule likely hindered co-engagement of both mechanisms of action (the Fc-mediated CD16a pathway and the NKp46-mediated pathway) required to augment tumor cell killing.

Discussion

Clic's single germline scaffold facilitated AI hit expansion

Clic's use of a single germline scaffold facilitated our AI-assisted hit expansion and successfully retrieved clones with an order of magnitude higher affinity than the 'seeds,' representing high-affinity clones from original selections. The VAE approach is agnostic to prior structural or functional knowledge of antibodies, relying solely on the observed sequence and activity data. This enables unbiased exploration of the sequence landscape and supports the discovery of diverse, functionally relevant antibody candidates beyond known motifs or germline constraints. Unlike rodents and most mammals, including humans, that use V(D)J (variable-diversity-joining) recombination as a primary mechanism to diversify their repertoires from the combinatorial assembly of multiple gene segments, the chicken is a single-scaffold species relying instead on gene conversion, starting with a functionally rearranged V(D)J gene[41]. Clic, an engineered chicken, leverages the chicken host's natural mechanisms of diversification. Our lineage definition allowed direct comparison of epitope diversity across Clic and Flic repertoires despite them reaching diversity in different ways: single scaffold versus multiple, combinatorially assembled scaffolds.

High throughput epitope binning uncovered nuanced and complementary diversity

Herein, we demonstrate that Clic and Flic repertoires provide complementary platforms for producing *in vivo*-optimized human immune repertoires for drug discovery, yielding high-affinity clones with cyno cross-reactivity, broad epitope coverage, and functional activity as NK engagers. In addition, our clones exhibited favorable developability properties when assessed by both *in-silico* and *in-vitro* methods (S5 Table). Our detailed epitope binning study revealed that both repertoires showed broad and complementary coverage, with most epitope communities being found in only one repertoire and not another, and few shared epitope communities. This intricate diversity can be appreciated in the community network plot (Figure 2b), the Venn diagram (Figure 4d) and Table 1, which collectively show the distribution of epitope communities within and across repertoires. We intersected our analysis with a small panel of literature benchmarks sourced from the immunization of mouse[32]. Flic was able to recapitulate their epitopes when analyzed at the epitope community level in our analysis. While Clic only recapitulated one of them (the Innate-2/9 epitope), Clic generated many Clic-unique epitope communities. This additional epitope coverage may reflect Clic's different recognition of human targets relative to mammalian host species (rodents) because the chicken is a divergent host species[42]. Both Clic and Flic expanded epitope coverage beyond the benchmarks and provided multiple cyno cross-reactive clones from different epitope communities (Figure 1c and S2 Table).

It is well-established that high throughput epitope binning assay can discriminate antibodies, aiding in the triage of large antibody panels to prioritize candidates for further study[43–45] and that the deduced epitope differences can be confirmed by structural methods[46–48], increasing confidence in binning assignments that may allow for the identification of antibodies with differentiated binding modes and unique mechanisms of actions. However, to fully appreciate the depth and breadth of epitope coverage contained in antibody repertoires, a few caveats must be met to optimize the information content of these assays. Not only are the choice and number of antibodies used for probing epitope coverage key but the 'granularity' of binning assignments is often a subjective exercise, relying on both good biosensor practices and statistically powered experimentation.

In Gauthier et al.'s assessment of 17 NKp46 clones, the authors observed that NKp46-2 (Innate-2) and NKp46-9 (Innate-9) cross-block one another but are non-identical because they can be differentiated by other antibodies (NKp46-8 and NKp46-12)[32] (see S2 Fig). While our study recapitulated their observation that Innate-1, 2/9, 3, and 4 target non-overlapping epitopes, we were unable to distinguish between Innate-2 (B02) and Innate-09 (B09) because we lacked such a discriminatory antibody, despite analyzing a much larger panel of (119) antibodies. This shows that, while increasing the number of antibodies in an epitope binning study increases the chances of finding antibodies that resolve epitope differences between highly similar epitopes, a smaller panel can suffice if they contain appropriate discriminatory power.

While we attempted an empirical full 119×119 pairwise competition of our multi-repertoire merged panel of clones, most clones (73%) did not regenerate as ligand when tested in a classical sandwich assay

format. Despite significant ligand attrition, we were still able to assign epitope communities to all antibodies in the study by relying on a core set of antibodies that performed well bidirectionally (as both analyte and ligand) and using them as ligands to probe a larger set of analyte-only tested clones. Our approach yielded precise epitope discrimination that was corroborated by epitope mapping data using HDX-MS, and our community assignments matched the granularity of sequence lineage assignments, further validating our approach. Com-4C1 mapped to residues *L39-F62*, Com-3 mapped to *H108-F121*, and Com-2a (all three members tested) was anchored by residues *L135-Y147* (Table 2).

Molecular format affects the potency of NK engagers

Our ADCC results showed that NKp46 antibodies from Clic and Flic targeting different epitopes could all reduce tumor cell growth to varying extents on a silent-Fc backbone, via a mechanism independent of the CD16a-mediated pathway. Format mattered, as LC-tethered scFv-IgGs appeared more potent than HC-tethered scFv-IgGs. Affinity did not seem to drive potency as C44, our highest affinity clone (with K_D value of 70 pM) was not the most potent, although it was only tested as an LC-tethered scFv-IgG, suggesting its potency may be improved if tested in an alternate, more optimum, format. Silenced Fc bispecifics could outperform their active Fc counterpart, suggesting that the molecular geometry could be optimized to favor co-engagement of both NK activation pathways (NKp46-mediated and CD16a/active-Fc-mediated). Indeed, molecular format, size, geometry, and valency are important factors that must be co-optimized in designing therapeutic NK engagers[12,39].

While the cmLC technology is conventionally used to simplify the generation of a 1 + 1 IgG-like format using a knobs-into-holes or similar Fc heterodimerization strategy, this study leveraged cmLC antibodies in an alternative configuration to create multivalent NK engagers. This approach was selected because multivalent formats are widely regarded as optimal for NK engagement, as supported by both literature and clinical evidence. Specifically, we utilized cmLC NKp46 antibodies to construct Morrison formats in which a benchmark anti-EGFR antibody (cetuximab) was incorporated as an scFv at various positions within a cmLC anti-NKp46 IgG backbone.

Notably, use of cmLC in a 1:1 IgG-like format necessitates that both target specificities (NKp46 and EGFR) be generated using the same cmLC platform. However, as this study focused exclusively on the discovery of novel NKp46 clones without a concurrent campaign against a tumor-associated target, we adopted an alternative strategy. We leveraged established ADCC assays using a commonly utilized EGFR-overexpressing cell line (A549, derived from a lung cancer patient) and incorporated cetuximab, a clinically validated benchmark antibody, to provide the EGFR-targeting component of the bispecific constructs.

The primary advantage of using cmLC antibodies in this context was the streamlined discovery process. Our single B-cell screening workflow concentrated solely on the heavy-chain variable domain, eliminating the need to maintain native LC-HC pairing, as all VH domains were inherently compatible with a single LC of known sequence.

In summary, our study demonstrates Clic and Flic as highly complementary antibody discovery platforms, each providing unique and synergistic contributions to sequence diversity, epitope diversity, and cross-species reactivity. The collective repertoires of Clic and Flic are impactful tools to generate next-generation NKp46 antibodies optimized for potent and tunable NK engagement.

Materials and methods

Trademark acknowledgements

OmniClic™ and OmnidAb® are trademarks of Crystal Bioscience, Inc.; OmniFlic® is a registered trademark of OmniAb, Inc.; xPloration® is a registered trademark of xCella Biosciences Inc.; and Hemlibra® is a registered trademark of Chugai Seiyaku Kabushiki Kasiha.

Immunizations and single B cell screening

Immunizations of OmniClic animals with human NKp46 and recovery of B cells were performed as described for OmnidAb animals[34]. The OmniFlic animals were subcutaneously immunized with the same

protein antigen in hock every 3–4 days for 6 weeks and B cells were recovered from lymph nodes instead of spleen. Single B cells were screened on the xPloration instrument, a microcapillary-based array screening system[33] using a bead-adsorbed protein target or a stable NKp46 CHO cell line (CHOK1-NKp46-Cell-Line, Kyinno Biotechnology, catalog number KC-1789). Hits were sequenced and unique-sequence clones were synthesized from custom-ordered DNA, expressed as full-length IgG1 and protein-A purified, prior to analytical characterization.

NGS processing

NGS data is preprocessed using pRESTO (0.7.1) from the Immcantation (Version 4.4.0) package and the resulting reliable antibody sequences from the preprocessing are annotated using IgBlast (1.18.0) that sources custom libraries for our OmniFlic- and OmniClic-derived antibodies. We then performed lineage analysis, clustering sequences with the same V and J gene, same heavy-chain CDR3 length, and an edit distance of two amino acids in the heavy-chain CDR3 region, to the annotated sequences from NGS libraries. When selecting clones, we first narrowed down to the lineages that contain both bead binders and cell binders from high throughput screening technique xPloration, reasoning that there is statistically high confidence in those lineages to bind with the target of interest. Clones are further selected using two methods. Method A selects clones based on the clone representation, picking the top and bottom 10 greatest representation clones from each overlap lineage. Method B selects clones that span across most lineages to capitalize on the diversity of the sequence space; the number of selected clones within each lineage is proportional to the size of the lineage. After selecting clones from both methods, we apply the liability assessment on both sequence and structural level to eliminate clones that have a high-risk developability issue.

Hit expansion

The data used for model building and selection included 69,000 unique heavy-chain amino acid sequences from NGS on three different OmniClic common light-chain chickens immunized with NKp46. Sequences were filtered for duplicate count greater than or equal to two. Activity data was provided for 178 unique amino acid sequences. Of the 178 sequences with activity data, 90 were inactive and the remaining 88 sequences had K_D values ranging from 2 to 500 nM. Error values for the 88 active sequences were obtained by propagating uncertainty for association and dissociation kinetic rate constants (k_a and k_d) from the SPR measurements. K_D values were scaled by -log2(K_D) with inactive values set to zero corresponding to a K_D 2000 nM. This placed all the activity data for regression in the range of 0 to 10.

Variational autoencoder model

Antibody sequences were modeled using a VAE model[49,50]. Input sequences were embedded using 1-hot encoding into a 21 × 134 matrix where 21 corresponds to the 20 standard amino acids plus an end character and 134 is the maximum sequence length. Encoding was performed using an LSTM layer with 134 nodes and dropout regularization followed by batch normalization. The size of the latent layer was 50 nodes and was modeled using a multivariate normal distribution from tensorflow-probability with learned variances and covariances. The prior was a N(0,1) distribution and KL weight was 0.75. The decoder layer consists of an upsampling dense layer of size 67 × 36 followed by a 1D deconvolutional layer with 18 filters and kernel size and strides of 2 and ReLU activation, and an LSTM layer with 134 nodes. Each of the preceding 3 layers in the decoder is followed by batch normalization. A final dense layer of 21 nodes[50] forms the model output. A Gaussian progress regression model also comes off the latent layer. This model has one dense variational layer with trainable prior and 1 node with ReLU activation followed by a Gaussian Process regression layer. Dropout regularization is applied off of the latent layer input to the regression layer. Overall, the Encoder has ~260K trainable parameters, the decoder has ~210K trainable parameters and the regression model has 230 trainable parameters for a total of ~470K trainable parameters.

Model training

Model training was performed for 500 epochs using a batch size of 500 using an Adam optimizer with Nesterov momentum with a learning rate of 0.002. The autoencoder and Gaussian progress regression models were trained simultaneously in one global model. Loss weights of 1 and 50 were applied to the reconstruction loss and Gaussian process log-likelihood loss, respectively.

Clone selection

Sequences were selected from the VAE model using the Expected Improvement (EI) Bayesian Optimization acquisition function. All sequences with an EI value greater than an internal reference set by sequences with a measured affinity <25 nM. Sequences were filtered for liabilities at the structural level. In this case, six homology models were generated per sequence using the Molecular Operating Environment (MOE) software. Mean and standard deviation of the standard descriptors used in MOE were computed across all six models and these values were used for filtering the selection.

Surface plasmon resonance

Binding kinetics (capture kinetics) and epitope binning (classical sandwich) experiments were conducted using a high-throughput SPR (HT-SPR) on Carterra's LSA platform equipped with HC30M as previously described[34]. Recombinant His-tagged human NKp46 protein was produced in-house (Uniprot Accession # O76036-1, residues 22 to 255) or sourced from Acro Biosystems (cat. no. NC1-H52H4) and recombinant His-tagged cyno NKp46 protein was sourced from Acro Biosystems (cat. no. NC1-C52H4). NKp46 proteins were polished by preparative size-exclusion chromatography (SEC) and monomeric fractions were isolated immediately prior to use. An anti-His mAb was used as a universal sandwiching control for all epitope binning experiments. Data were processed, analyzed, and figures generated using the Carterra EP™ software. Clones that performed as both ligand and analyte were amenable to a fully comprehensive bidirectional analysis, whereas clones that failed as ligand, were tested as analyte-only and therefore were not tested for mutual competition. To simulate a full heat map to facilitate hierarchical clustering into epitope communities, the blocking data from the 119 × 33 'many-on-few' analyte-on-ligand heat map was used to infer 'missing' data (for analyte-only clones lacking a ligand counterpart) by transposing the measured blocking results (block or not block) and assuming a fully symmetrical pairwise competition matrix. The 'inferred' reconstructed heat map was then subjected to a user-defined cut-height to generate 14 epitope 'communities' (S3 Fig).

HDX-MS epitope mapping

Samples for HDX-MS analysis were named as follows: Sample-7 (F31), Sample-8 (F23), Sample-10 (C24), Sample-11 (C08), Sample-12 (C70), Sample-13 (C65), and Sample-15 (D01). Sample-7 to Sample-12 were analyzed in a separate experiment than Sample-13 and Sample-15. In-house-produced NKp46 was used for the HDX-MS experiments.

Sample preparation

HDX reactions comparing apo NKp46 to NKp46 incubated with Sample-7 to Sample-12 were carried out in a 10 µl reaction volume containing 30 pmol of NKp46 and 30 pmol of Sample-7 to Sample-12. The exchange reactions were initiated by the addition of 7.8 µL of D2O buffer (50 mM HEPES pH 7.5, 150 mM NaCl, 92.6% D2O (V/V)) to 2.2 µL of protein (final D2O concentration of 72.3%). HDX reactions comparing apo NKp46 to NKp46 incubated with Sample-13 and Sample-15 were carried out in a 15 µl reaction volume containing 30 pmol of NKp46 and 30 pmol of Sample-13 or Sample-15. The exchange reactions were initiated by the addition of 11.8 µL of D2O buffer (50 mM HEPES pH 7.5, 150 mM NaCl, 92.6% D2O (V/V)) to 3.2 µL of protein (final D2O concentration of 72.8%). Reactions proceeded for 10s, 100s, 1000s and 10000s at 20°C before being quenched with ice cold acidic quench

buffer, resulting in a final concentration of 0.6 M guanidine HCl and 0.9% formic acid post quench. All conditions and timepoints were created and run in independent triplicate. Samples were flash frozen immediately after quenching and stored at −80°C until injected onto the ultra-performance liquid chromatography (UPLC) system for proteolytic cleavage, peptide separation, and injection onto a QTOF or Orbitrap for mass analysis, described below.

Protein digestion and MS/MS data collection

Protein samples were rapidly thawed and injected onto an integrated fluidics system containing a HDx-3 PAL liquid handling robot and climate-controlled (2°C) chromatography system (LEAP Technologies), a Waters Acquity UPLC I-Class Series System, as well an Orbitrap Exploris 120 Mass Spectrometer (ThermoFisher). The full details of the automated LC system were previously described[51]. The samples were run over an immobilized pepsin column (Affipro; AP-PC-001) at 200 µL/min for 4 minutes at 2°C. The resulting peptides were collected and desalted on a C18 trap column (Acquity UPLC BEH C18 1.7 µm column (2.1 × 5 mm); Waters 186,004,629). The trap was subsequently eluted in line with an ACQUITY 300Å, 1.7 µm particle, 100 × 2.1 mm BEH C18 UPLC column (Waters), using a gradient of 3–10% B (Buffer A 0.1% formic acid; Buffer B 100% acetonitrile) over 1.5 minutes, followed by a gradient of 10–25% B over 4.5 minutes, followed by a gradient of 25–35% B over 5 minutes, finally, after 1 minute, at 35% B a gradient of 35–80% B over 1 minute was used. MS experiments acquired over a mass range from 150 to 2200 m/z using an electrospray ionization source operated at a temperature of 200°C and a spray voltage of 4.5 kV. Same LC system, gradient and columns were used for all samples.

Peptide identification

Peptides were identified from the non-deuterated samples of NKp46 using data-dependent acquisition following tandem MS/MS experiments (precursor scan from 300 to 1500 m/z, 4 data dependent scans from 300 to 1500 m/z, dynamic exclusion set to $n = 1$ with 10s exclusion time, 6s expected LC peak width on Orbitrap system). MS/MS datasets were analyzed using FragPipe v18.0 and peptide identification was carried out by using a false discovery-based approach using a database of purified proteins and known contaminants[52–54]. MSFragger was utilized, and the precursor mass tolerance error was set to −20 to 20 ppm. The fragment mass tolerance was set at 20ppm. Protein digestion was set as nonspecific, searching between lengths of 4 and 50 aa, with a mass range of 400 to 5000 Da.

Mass analysis of peptide centroids and measurement of deuterium incorporation

HD-Examiner Software (Sierra Analytics) was used to automatically calculate the level of deuterium incorporation into each peptide. All peptides were manually inspected for, for example, correct charge state, correct retention time, and appropriate selection of isotopic distribution. Deuteration levels were calculated using the centroid of the experimental isotope clusters. Results are presented as relative levels of deuterium incorporation and the only control for back exchange was the level of deuterium present in the buffer (72.3% or 72.8%). Differences in exchange in a peptide were considered significant if they met all three of the following criteria: ≥5% change in exchange, ≥0.4 Da difference in exchange, and a p value <0.01 using a two-tailed student T-test. Samples were only compared within a single experiment and were never compared to experiments completed at a different time with a different final D2O level. The data analysis statistics for all HDX-MS experiments are in S3 Table according to published guidelines[55] (see S1 File for the source data file). The MS proteomics data have been deposited to the ProteomeXchange Consortium via the PRIDE partner repository[56] with the dataset identifier (PXD069455).

In-vitro developability assessment of anti-NKp46 antibodies

Thermal stability (Tm) and aggregation (Tagg) were determined by differential scanning fluorimetry (UNCLE-0330, Unchained Labs); and homogeneity and purity were assessed by analytical SEC as described previously[34].

Generation of antibody models and in silico assessment of potential liabilities and post-translational modifications

For each of the eight clone sequences of interest (F15, F23, F31, C08, C24, C44, C65, C70), 25 Fv models were generated using Antibody modeler in MOE[57]. In all cases, a maximum of five different frameworks and five different CDR combinations of structural templates were used. All models generated were then subjected to energy minimization prior to structure-based annotation of potential post-translational modifications and liabilities. Liability score A, derived from previous work by Thorsteinson et al.[58], was calculated for each model. It reflects the presence of exposed high-risk Asn deamidation and Asp isomerization motifs in the CDRs or framework, potential glycosylation sites within the CDRs, total CDR length, Fc total charge, VH-VL absolute charge difference, and size of CDR hydrophobic patch areas. We also used these models to evaluate potential unpaired cysteines in the CDRs and aggregation prone motifs (none to be reported), as well as to calculate the average isoelectric point (pI) and net charge at neutral pH[57].

Production of bispecific antibodies for ADCC

Clones C08, C44, and F15 were selected for reformatting into a symmetrical tetravalent 2 + 2 scFv-IgG Morrison format using cetuximab scFv tethered from the C-terminal of the heavy chain (HC) or light chain (LC) of NKp46 Clic or Flic IgG backbone. Constructs were prepared in pairs: one construct had an active IgG1-Fc, the other incorporated STR silencing mutations[59]. Plasmids were constructed by following the manufacturer's protocol of Gibson Assembly® Cloning Kit (NEB, E5510S) and amplified with EndoFree Plasmid Maxi Kit (Qiagen, 12,362). Proteins were expressed in HEK293 cells and protein-A purified followed by preparative SEC (Fig. S5c and S5d).

Antibody-dependent cellular cytotoxicity assay

A 2D ADCC assay was performed by Charles River Laboratories, Inc. using the IncuCyte Live-Cell Analysis System for continuous visualization and automated analysis of immune cell-mediated killing of tumor cells (Sartorius, Inc). Donor-derived NK cells and EGFR-expressing target cells (A549) were used to test a panel of eight NKp46 X EGFR bispecific compounds, representing two Morrison formats. Six total donors were used, split into cohorts of three donors per Morrison format (to test four compounds per set of three donors) and each experimental condition was tested in triplicate. Each immune-assay readout was performed once. Readouts were tumor cell growth over time by IncuCyte.

The ADCC assay comprised 4 steps: target cell seeding, CD56-positive cells isolation, tumor killing assay, and data analysis, as follows. NucLight Red (NLR) expressing A549 cells were cultured under standard aseptic conditions. On day −1 these cells were seeded into Poly-L-Lysine coated 96-well plates at $7.5x10^3$ cells/well. Human peripheral blood mononuclear cells (PBMCs) were isolated from three healthy donors via density gradient separation. CD56+ NK cells were isolated from PBMCs by magnetic separation and CD56 purity was confirmed by flow cytometry prior to co-culture with target A549 tumor cells. Following CD56+ cell isolation, NK cells were incubated with target tumor cells expressing the NucLight Red (NLR) nuclear dye at a 10:1 effector:target (E:T) ratio. Co-cultures were incubated with 20 µg/mL bispecific compounds. Appropriate controls were included: tumor cells alone, tumor cells/NKs in the presence of 20 µg/ml Cetuximab (IgG1 targeting EGFR Control), 20 µg/ml IgG1 isotype control, 1 µM bortezomib (cytotoxic control) or 10 ng/ml IL-2+IL-12+IL-15 (NK activation positive control). Tumor cell growth was determined as the total red count (A549 NLR cells) per well normalized to $T = 0$. Area under curve (AUC) growth data was calculated in GraphPad Prism and reported as mean ± SEM (shown as error bars) of triplicate biological replicates. All samples were compared with untreated or vehicle (PBS alone): see S2 File for statistical T-tests.

Acknowledgements

JEB is supported by the Natural Science and Engineering Research Council (Discovery Grant NSERC-2020–04241). We would like to thank Diego Espinosa, Manith Norng, and Kathryn Randene (OmniAb, Inc) for their assistance in

producing the human NKp46 protein and antibody samples used in this study. We also would like to thank Marie Carkill, Becky Longley, Will Morley, and Elsenoor Klaver (Charles River Laboratories International, Inc) for their helpful discussions about the ADCC data.

Disclosure statement

No potential conflict of interest was reported by the author(s).

Funding

The work was supported by the Natural Sciences and Engineering Research Council of Canada [NSERC-2020-04241].

ORCID

Baisen Zeng http://orcid.org/0000-0002-7780-3501
Ingrid Mechin http://orcid.org/0000-0001-6939-4886
David Mowrey http://orcid.org/0000-0002-4413-9384
Gerry S Rivera http://orcid.org/0000-0003-4781-8523
Hunter G Nyvall http://orcid.org/0009-0006-0098-0688
Sushant Suresh http://orcid.org/0009-0005-7220-7339
John E Burke http://orcid.org/0000-0001-7904-9859
William Harriman http://orcid.org/0009-0009-5015-8256
Bob Chen http://orcid.org/0009-0002-5792-0935
Yasmina Abdiche http://orcid.org/0009-0001-8611-2438

Author contributions

BZ, IM, DM, GSR, WH, BC, and YA are employees and shareholders of OmniAb, Inc.

Conceptualization: YA BZ; Investigation: BZ HGN SS; Formal Analysis: YA BZ IM HGN SS JEB; Project Administration: YA; Resources: GSR; Software: BC, DM; Writing – Original Draft Preparation: YA BZ IM DM; Writing – Review & Editing: BC WH YA BZ.

References

1. Chan AC, Martyn GD, Carter PJ. Fifty years of monoclonals: the past, present and future of antibody therapeutics. Nat Rev Immunol. 2025;25(10):745–765. doi: 10.1038/s41577-025-01207-9
2. Crescioli S, Kaplon H, Wang L, Visweswaraiah J, Kapoor V, Reichert JM. Antibodies to watch in 2025. mAbs. 2025;17(1). doi: 10.1080/19420862.2024.2443538
3. Kothari M, Wanjari A, Acharya S, Karwa V, Chavhan R, Kumar S, Kadu A, Patil R. A comprehensive review of monoclonal antibodies in modern medicine: tracing the evolution of a revolutionary therapeutic approach. Cureus. 2024; doi: 10.7759/cureus.61983
4. Castelli MS, McGonigle P, Hornby PJ. The pharmacology and therapeutic applications of monoclonal antibodies. Pharmacol Res Perspect. 2019;7(6). doi: 10.1002/prp2.535
5. Carter PJ, Rajpal A. Designing antibodies as therapeutics. Cell. 2022;185(15):2789–2805. doi: 10.1016/j.cell.2022.05.029
6. Surowka M, Klein C. A pivotal decade for bispecific antibodies? mAbs. 2024;16(1). doi: 10.1080/19420862.2024.2321635
7. Choi SM, Lee J-H, Ko S, Hong S-S, Jin H-E. Mechanism of action and pharmacokinetics of approved bispecific antibodies. Biomol Ther. 2024;32(6):708–722. doi: 10.4062/biomolther.2024.146
8. Guidi L, Etessami J, Valenza C, Valdivia A, Meric-Bernstam F, Felip E, Curigliano G. Bispecific antibodies in hematologic and solid tumors: current landscape and therapeutic advances. Am Soc Clin Oncol Educ Book. 2025;45(3). doi: 10.1200/EDBK-25-473148
9. Elshiaty M, Schindler H, Christopoulos P. Principles and current clinical landscape of multispecific antibodies against cancer. Int J Mol Sci. 2021;22(11):5632. doi: 10.3390/ijms22115632
10. Keri D, Walker M, Singh I, Nishikawa K, Garces F. Next generation of multispecific antibody engineering. Antibody Ther. 2024;7(1):37–52. doi: 10.1093/abt/tbad027
11. Goebeler M-E, Stuhler G, Bargou R. Bispecific and multispecific antibodies in oncology: opportunities and challenges. Nat Rev Clin Oncol. 2024;21(7):539–560. doi: 10.1038/s41571-024-00905-y

12. Zhu A, Bai Y, Nan Y, Ju D. Natural killer cell engagers: from bi-specific to tri-specific and tetra-specific engagers for enhanced cancer immunotherapy. Clin Transl Med. 2024;14(11). doi: 10.1002/ctm2.70046
13. Kassner J, Abdellatif B, Yamshon S, Monge J, Kaner J. Current landscape of CD3 bispecific antibodies in hematologic malignancies. Trends Cancer. 2024;10(8):708–732. doi: 10.1016/j.trecan.2024.06.001
14. Shanshal M, Caimi PF, Adjei AA, Ma WW. T-cell engagers in solid cancers—current landscape and future directions. Cancers. 2023;15(10):2824. doi: 10.3390/cancers15102824
15. Shan KS, Din SMU, Dalal S, Gonzalez T, Dalal M, Ferraro P, Hussein A, Vulfovich M. Bispecific antibodies in solid tumors: advances and challenges. Int J Mol Sci. 2025;26(12):5838. doi: 10.3390/ijms26125838
16. Lloyd K, Middelburg J, Ovcinnikovs V, Pencheva N, Kemper K, Hall TV. Improving CD3 bispecific antibody therapy in solid tumors using combination strategies. Front Oncol. 2025;15. doi: 10.3389/fonc.2025.1548446
17. Middelburg J, Kemper K, Engelberts P, Labrijn AF, Schuurman J, Hall TV. Overcoming challenges for CD3-bispecific antibody therapy in solid tumors. Cancers. 2021;13(2):287. doi: 10.3390/cancers13020287
18. Zaïr ZM, Butterworth G, Shalaby M, Oštarijaš E, Thisthlethwaite F. T-cell engager toxicity in clinical phase trials; a systematic review and meta-analysis. Cancer Treat Rev. 2025;139:102991. doi: 10.1016/j.ctrv.2025.102991
19. Bergamaschi C, Gaspar M, Ciucci T, Sitnikova SI, Cayatte C, Pica M, Dovedi SJ. Innovative strategies for T cell engagers for cancer immunotherapy. mAbs. 2025;17(1). doi: 10.1080/19420862.2025.2531223
20. Huan T, Guan B, Li H, Tu X, Zhang C, Tang B. Principles and current clinical landscape of NK cell engaging bispecific antibody against cancer. Hum Vaccines Immunother. 2023;19(2). doi: 10.1080/21645515.2023.2256904
21. Shin MH, Oh E, Minn D. Current developments in NK cell engagers for cancer immunotherapy: focus on CD16A and NKp46. Immune Network. 2024;24(5). doi: 10.4110/in.2024.24.e34
22. Pinto S, Pahl J, Schottelius A, Carter PJ, Koch J. Reimagining antibody-dependent cellular cytotoxicity in cancer: the potential of natural killer cell engagers. Trends Immunol. 2022;43(11):932–946. doi: 10.1016/j.it.2022.09.007
23. Merchant AM, Zhu Z, Yuan JQ, Goddard A, Adams CW, Presta LG, Carter P. An efficient route to human bispecific IgG. Nat Biotechnol. 1998;16(7):677–681. doi: 10.1038/nbt0798-677
24. Brinkmann U, Kontermann RE. The making of bispecific antibodies. mAbs. 2017;9(2):182–212. doi: 10.1080/19420862.2016.1268307
25. Blarcom TV, Lindquist K, Melton Z, Cheung WL, Wagstrom C, McDonough D, Oseguera CV, Ding S, Rossi A, Potluri S, et al. Productive common light chain libraries yield diverse panels of high affinity bispecific antibodies. mAbs. 2018;10(2):256–268. doi: 10.1080/19420862.2017.1406570
26. Hermans C, Pierce GF. Bispecific antibodies mimicking factor VIII in hemophilia A: converting innovation to an essential medicine. Res Pract Thromb Haemost. 2023;7(4):100173. doi: 10.1016/j.rpth.2023.100173
27. You G, Won J, Lee Y, Moon D, Park Y, Lee SH, Lee S-W. Bispecific antibodies: a smart arsenal for cancer immunotherapies. Vaccines. 2021;9(7):724. doi: 10.3390/vaccines9070724
28. Lundberg AS, Geuijen CAW, Hill S, Bueren JJLV, Fumagalli A, Kruif JD, Silverman PB, Tabernero J. Petosemtamab, a bispecific antibody targeting epidermal growth factor receptor (EGFR) and leucine-rich G repeat-containing protein-coupled receptor (LGR5) designed for broad clinical applications. Cancers. 2025;17(10):1665. doi: 10.3390/cancers17101665
29. Ching KH, Berg K, Reynolds K, Pedersen D, Macias A, Abdiche YN, Harriman WD, Leighton PA. Common light chain chickens produce human antibodies of high affinity and broad epitope coverage for the engineering of bispecifics. mAbs. 2021;13(1). doi: 10.1080/19420862.2020.1862451
30. Buelow B, Choudry P, Clarke S, Dang K, Davison L, Aldred SF, Harris K, Pratap P, Pham D, Rangaswamy U, et al. Pre-clinical development of TNB-383B, a fully human T-cell engaging bispecific antibody targeting BCMA for the treatment of multiple myeloma. J Clin Oncol. 2018;36(15_suppl):8034. doi: 10.1200/JCO.2018.36.15_suppl.8034
31. Malik-Chaudhry HK, Prabhakar K, Ugamraj HS, Boudreau AA, Buelow B, Dang K, Davison LM, Harris KE, Jorgensen B, Ogana H, et al. Tnb-486 induces potent tumor cell cytotoxicity coupled with low cytokine release in preclinical models of B-NHL. mAbs. 2021;13(1). doi: 10.1080/19420862.2021.1890411
32. Gauthier L, Morel A, Anceriz N, Rossi B, Blanchard-Alvarez A, Grondin G, Trichard S, Cesari C, Sapet M, Bosco F, et al. Multifunctional natural killer cell engagers targeting NKp46 trigger protective tumor immunity. Cell. 2019;177(7):1701–1713. doi: 10.1016/j.cell.2019.04.041
33. Chen B, Lim S, Kannan A, Alford SC, Sunden F, Herschlag D, Dimov IK, Baer TM, Cochran JR. High-throughput analysis and protein engineering using microcapillary arrays. Nat Chem Biol. 2016;12(2):76–81. doi: 10.1038/nchembio.1978
34. Vuong CN, Reynolds KM, Rivera GS, Zeng B, Karimpourkalou Z, Norng M, Zhang Y, Chowdhury R, Pedersen D, Pantoja M, et al. Heavy chain-only antibodies with a stabilized human VH in transgenic chickens for therapeutic antibody discovery. mAbs. 2024;16(1). doi: 10.1080/19420862.2024.2435476
35. Vorauer C, Boniche-Alfaro C, Murphree T, Matsui T, Weiss T, Fries BC, Guttman M. Direct mapping of polyclonal epitopes in serum by HDX-MS. Analytical Chem. 2024;96(42):16758–16767. doi: 10.1021/acs.analchem.4c03274

36. Ständer S, Grauslund LR, Scarselli M, Norais N, Rand K. Epitope mapping of polyclonal antibodies by hydrogen–deuterium exchange mass spectrometry (HDX-MS). Analytical Chem. 2021;93(34):11669–11678. doi: 10.1021/acs.analchem.1c00696
37. Calvaresi V, Redsted A, Norais N, Rand KD. Hydrogen–deuterium exchange mass spectrometry with integrated size-exclusion chromatography for analysis of complex protein samples. Analytical Chem. 2021;93(33):11406–11414. doi: 10.1021/acs.analchem.1c01171
38. Coloma MJ, Morrison SL. Design and production of novel tetravalent bispecific antibodies. Nat Biotechnol. 1997;15(2):159–163. doi: 10.1038/nbt0297-159
39. Nikkhoi SK, Li G, Hatefi A. Natural killer cell engagers for cancer immunotherapy. Front Oncol. 2025;14. doi: 10.3389/fonc.2024.1483884
40. Lee RB, Maddineni S, Landry M, Diaz C, Tashfeen A, Yamada-Hunter SA, Mackall CL, Beinat C, Sunwoo JB, Cochran JR. An engineered NKp46 antibody for construction of multi-specific NK cell engagers. Protein Eng, Des Selection. 2024;37. doi: 10.1093/protein/gzae013
41. Mallaby J, Mwangi W, Ng J, Stewart A, Dorey-Robinson D, Kipling D, Hershberg U, Fraternali F, Nair V, Dunn-Walters D. Diversification of immunoglobulin genes by gene conversion in the domestic chicken (*Gallus gallus* domesticus). Discov Immunol. 2023;2(1). doi: 10.1093/discim/kyad002
42. Banik SSR, Kushnir N, Doranz BJ, Chambers R. Breaking barriers in antibody discovery: harnessing divergent species for accessing difficult and conserved drug targets. mAbs. 2023;15(1). doi: 10.1080/19420862.2023.2273018
43. Sivasubramanian A, Estep P, Lynaugh H, Yu Y, Miles A, Eckman J, Schutz K, Piffath C, Boland N, Niles RH, et al. Broad epitope coverage of a human in vitro antibody library. mAbs. 2017;9(1):29–42. doi: 10.1080/19420862.2016.1246096
44. Abdiche YN, Miles A, Eckman J, Foletti D, Blarcom TJV, Yeung YA, Pons J, Rajpal A. High-throughput epitope binning assays on label-free array-based biosensors can yield exquisite epitope discrimination that facilitates the selection of monoclonal antibodies with functional activity. PLOS ONE. 2014;9(3):e92451. doi: 10.1371/journal.pone.0092451
45. Wec AZ, Haslwanter D, Abdiche YN, Shehata L, Pedreño-Lopez N, Moyer CL, Bornholdt ZA, Lilov A, Nett JH, Jangra RK, et al. Longitudinal dynamics of the human B cell response to the yellow fever 17D vaccine. Proc Natl Acad Sci. 2020;117(12):6675–6685. doi: 10.1073/pnas.1921388117
46. Hastie KM, Li H, Bedinger D, Schendel SL, Dennison SM, Li K, Rayaprolu V, Yu X, Mann C, Zandonatti M, et al. Defining variant-resistant epitopes targeted by SARS-CoV-2 antibodies: a global consortium study. Science. 2021;374(6566):472–478. doi: 10.1126/science.abh2315
47. Yeung YA, Foletti D, Deng X, Abdiche Y, Strop P, Glanville J, Pitts S, Lindquist K, Sundar PD, Sirota M, et al. Germline-encoded neutralization of a Staphylococcus aureus virulence factor by the human antibody repertoire. Nat Commun. 2016;7(1). doi: 10.1038/ncomms13376
48. Sim J, Sockolosky JT, Sangalang E, Izquierdo S, Pedersen D, Harriman W, Wibowo AS, Carter J, Madan A, Doyle L, et al. Discovery of high affinity, pan-allelic, and pan-mammalian reactive antibodies against the myeloid checkpoint receptor SIRPα. mAbs. 2019;11(6):1036–1052. doi: 10.1080/19420862.2019.1624123
49. Hawkins-Hooker A, Depardieu F, Baur S, Couairon G, Chen A, Bikard D. Generating functional protein variants with variational autoencoders. PLoS Comput Biol. 2021;17(2):e1008736. doi: 10.1371/journal.pcbi.1008736
50. Kingma PD, Welling M. Auto-encoding variational Bayes. arXiv:1312.6114. 2013. doi: 10.48550/arXiv.1312.6114
51. Stariha JTB, Hoffmann RM, Hamelin DJ, Burke JE. Probing protein–membrane interactions and dynamics using hydrogen–deuterium exchange mass spectrometry (HDX-MS). Methods Mol Biol. 2021; 465–485. doi: 10.1007/978-1-0716-1197-5_22
52. Kong AT, Leprevost FV, Avtonomov DM, Mellacheruvu D, Nesvizhskii AI. Msfragger: ultrafast and comprehensive peptide identification in mass spectrometry–based proteomics. Nat Methods. 2017;14(5):513–520. doi: 10.1038/nmeth.4256
53. Dobbs JM, Jenkins ML, Burke JE. Escherichia coli and Sf9 contaminant databases to increase efficiency of tandem mass spectrometry peptide identification in structural mass spectrometry experiments. J Am Soc Mass Spectrom. 2020;31(10):2202–2209. doi: 10.1021/jasms.0c00283
54. Leprevost FDV, Haynes SE, Avtonomov DM, Chang H-Y, Shanmugam AK, Mellacheruvu D, Kong AT, Nesvizhskii AI. Philosopher: a versatile toolkit for shotgun proteomics data analysis. Nat Methods. 2020;17(9):869–870. doi: 10.1038/s41592-020-0912-y
55. Masson GR, Burke JE, Ahn NG, Anand GS, Borchers C, Brier S, Bou-Assaf GM, Engen JR, Englander SW, Faber J, et al. Recommendations for performing, interpreting and reporting hydrogen deuterium exchange mass spectrometry (HDX-MS) experiments. Nat Methods. 2019;16(7):595–602. doi: 10.1038/s41592-019-0459-y
56. Perez-Riverol Y, Bai J, Bandla C, García-Seisdedos D, Hewapathirana S, Kamatchinathan S, Kundu D, Prakash A, Frericks-Zipper A, Eisenacher M, et al. The pride database resources in 2022: a hub for mass spectrometry-based proteomics evidences. Nucleic Acids Res. 2022;50(D1):D543–D552. doi: 10.1093/nar/gkab1038
57. Maier JKX, Labute P. Assessment of fully automated antibody homology modeling protocols in molecular operating environment. Proteins: Struct Func Bioinf. 2014;82(8):1599–1610. doi: 10.1002/prot.24576

58. Thorsteinson N, Gunn JR, Kelly K, Long W, Labute P. Structure-based charge calculations for predicting isoelectric point, viscosity, clearance, and profiling antibody therapeutics. mAbs. 2021;13(1). doi: 10.1080/19420862.2021.1981805
59. Wilkinson I, Anderson S, Fry J, Julien LA, Neville D, Qureshi O, Watts G, Hale G. Fc-engineered antibodies with immune effector functions completely abolished. PLOS ONE. 2021;16(12):e0260954. doi: 10.1371/journal.pone.0260954